Rock Dynamics: From Research to Engineering – Li et al. (Eds)
© 2016 Taylor & Francis Group, London, ISBN 978-1-138-02953-8

Microseismic energy evolution of high rock slop during excavation and after reinforcement

D.Y. Zhuang, Z.Z. Liang & C.A. Tang
Institute of Rock Instability and Seismicity Research, Dalian University of Technology, China

K. Ma
Institute of Mechanics, Chinese Academy of Sciences, China

ABSTRACT: Rock mass is known to exchange energy with the external environment when it is under load until it fails, a destabilization phenomenon driven by energy. In order to investigate the energy evolution of high rock slope and its relation with rock mass failure of the slope during slope excavation and after reinforcement, a parameter called microseismic energy density was proposed and the relationship between microseismic energy density and the stress and strain of rock mass was discussed. Taking right bank slope of the Dagangshan Hydropower station as an example, the microseismic energy release and energy transference of rock mass during slope excavation and after reinforcement were revealed. These lead to conclusions: Firstly, not only the distribution and intensity of microseismicity but also the potential dangerous area of the slope can be determined synthetically by microseismic energy density. Secondly, the distribution of high energy release zones is closely related to the locations of the deep unloading fracture zones XL_{316-1} and the fault f_{231} moderately dipping out of the slope. Finally, the microseismic event rate and energy density decreased significantly after reinforcing, and the relative high energy release zones transferred to the edge of anti-shear tunnels and low-threat faults, dikes in the deeper area of the slope, so its mechanical behavior was obviously improved. Conclusions can provide references for developing energy criterion and the prediction method of high rock slope failure.

1 INTRODUCTION

Rock mass is under external loading, it either absorbs external energy (e.g., mechanical energy and thermal energy) or converts it to its own internal energy or releases its internal strain energy in a certain form until it fails. This is an energy-driven destabilization phenomenon (Xie et al. 2008). Energy evolution during rock deformation and failure can be mainly divided into four processes: energy input, energy accumulation, energy dissipation and energy release (Zhang et al. 2015). Many studies concentrated on energy evolution patterns of rock through theoretical and experimental studies. Zhang & Gao (2015) studied the confining pressure effects on variation and allocation pattern of elastic energy and dissipated energy by conducting axial loading and unloading tests under six different confining pressures for sandstone samples. In order to determine the relationship between energy transformation and coal failure, Peng et al. (2015) investigated the mechanical behaviors of coal specimens taken from a 600-m deep mine conventional triaxial compression tests using five different confining pressures. In engineering practice, Murphy et al. (2012) investigated the relative radiated seismic energy of the explosion by collecting seismic signatures from underground explosions. Zhang et al. (2013) offered a method for hazard assessment in mines, which is based on seismic energy release distribution. Thus, energy release, also seismic radiated energy provides a practical index for evaluating the stability of rock mass structures, including high rock slope. However, little research focused on the relationship between monitoring energy release and stress and strain of rock, an important mechanical concept for assessing the slope stability,

which hinders the stability evaluation of engineering rock masses using microseismic monitoring technique. Meanwhile, with high rock slope widely used, it is necessary to develop stability evaluation and failure prediction methods based on energy monitored which is more available and authentic than theoretical analysis.

In this study, a parameter called microseismic energy density comprehensively reflecting the location and intensity of micro-cracking in rock mass was proposed and the relationship between microseismic energy density and the stress and strain of rock mass was discussed. Using microseismic monitoring data of right bank slope of the Dagangshan Hydropower station, the microseismic energy release and energy transference patterns of rock mass in high rock slope during slope excavation and after reinforcement were revealed.

2 MICROSEISMIC ENERGY DENSITY

The elastic energy in rock mass is transformed into inelastic strain energy during fracturing and sliding. Other than the energy dissipated by fracturing and seismic wave propagation, the remaining energy is the microseismic radiation energy received by the sensors. As a measurement for the intensity of microseismic events, the microseismic radiation energy is widely used in studies on microseismic activity for mines (Snelling et al. 2013). According to the studies by Boatwright & Fletcher (1984), the microseismic energy of the seismic source can be calculated from the monitored body wave (P-wave and S-wave):

$$E = 4\pi\rho c R^2 \frac{J_c}{F_c^2} \tag{1}$$

where E is the microseismic energy, ρ is the rock mass density, c is the body wave velocity of the seismic source, R is the distance between the seismic source and sensor, J_c is the energy flux, which can be obtained by integration of particle velocity spectra in the frequency domain, and F_c is the empirical coefficient for the type of seismic wave radiation, which is 0.52 and 0.63 for P-wave and S-wave, respectively (Aki & Richards, 1980). The total energy of the two body waves is the microseismic energy.

For a particular micro-crack, called microseismic event in rock engineering, Source volume, the volume of coseismic inelastic deformation that radiated the recorded seismic waves can be estimated from

$$V = M / \Delta\sigma \tag{2}$$

where M is the seismic moment of microseismic events and $\Delta\sigma$ is the stress drop of the microseismic source before and after micro-cracking.

Since apparent stress σ_A scales with stress drop and there is less model dependence in determining the apparent stress than there is in determining corner frequency cubed dependent static stress drop, the apparent volume V_A can be defined as follows (Mendecki 1997):

$$V_A = \frac{M}{2\sigma_A} = \frac{M}{2\mu E} \tag{3}$$

where μ is the stiffness of rock mass. The apparent volume for a given microseismic event measures the volume of rock with coseismic inelastic strain with accuracy in the order of magnitude of apparent stress divided by rigidity.

The microseismic energy density can be defined as follows:

$$E_d = E / V_A \tag{4}$$

Substituting Eq. 3 into Eq. 4, and assuming that the apparent strain of seismic source is equal to the strain change, we have:

$$E_d = 2\sigma_A \cdot \varepsilon_A \approx \Delta\sigma \cdot \Delta\varepsilon \tag{5}$$

As the energy release during micro-cracking in unit volume of rock mass, the microseismic energy density can not only comprehensively reflect the location and intensity of micro-cracking in rock mass, but also represent the strain energy storage and release process of rock masses in the microseismic source zone. Meanwhile, it can be used to investigate the state of engineering rock mass under external disturbances. The high energy density zone in the slope corresponds to the high energy release zone, and also the micro-cracking concentration and rock damage zone after the rock mass strength is reached.

3 MICROSEISMIC ENERGY EVOLUTION OF HIGH ROCK SLOPE

3.1 *Project overview*

This case study is the right bank slope of Dagangshan Hydropower Station, which is located at Dadu River in Wajiao Township, Shimian County, Sichuan Province, southwest China. As a typical deep "Ω"-shaped valley, the slopes have experienced long-term epigenetic reformation. As a result, a great amount of diabase and granite aplite dikes are developed in the slope, which are fractured and have poor mechanical properties. The existence of structural planes (such as XL_{316-1}, XL_{9-15} and f_{231}) dipping out of slope lead to reduced rock mass strength and integrity, and results in anisotropy of rock masses. The slope is featured by large slope angles, complex geological conditions and outstanding stability problems (Fig. 1).

Obvious local deformation and failure was observed on the slope surface during excavation due to complex rock mass structures, and the slope excavation is forced to stop at elevation 1070 m because of instable large rock blocks (Ma 2014). For an extremely large-scale controlling structure with specific boundaries and prone to failure, anti-shear tunnels were adopted to replace weak structures with micro-expansion concrete so as to control the continuing slope deformation. After completing excavation and backfill of the lower 3 anti-shear tunnels in June 2010, slope excavation was restored and the elevation of slope excavation extended to 917 m in June 2011. The excavation of anti-shear tunnels and slope were finished before 30 September 2011, and reinforcement by anti-shear tunnels was fully done until November 2011.

3.2 *Distribution of microseismic energy release during excavation*

Figure 2 shows the temporal distribution of elevation of excavation and accumulative microseismic energy from 4 May 2010 to 31 May 2012. Without regard to the failure of monitoring

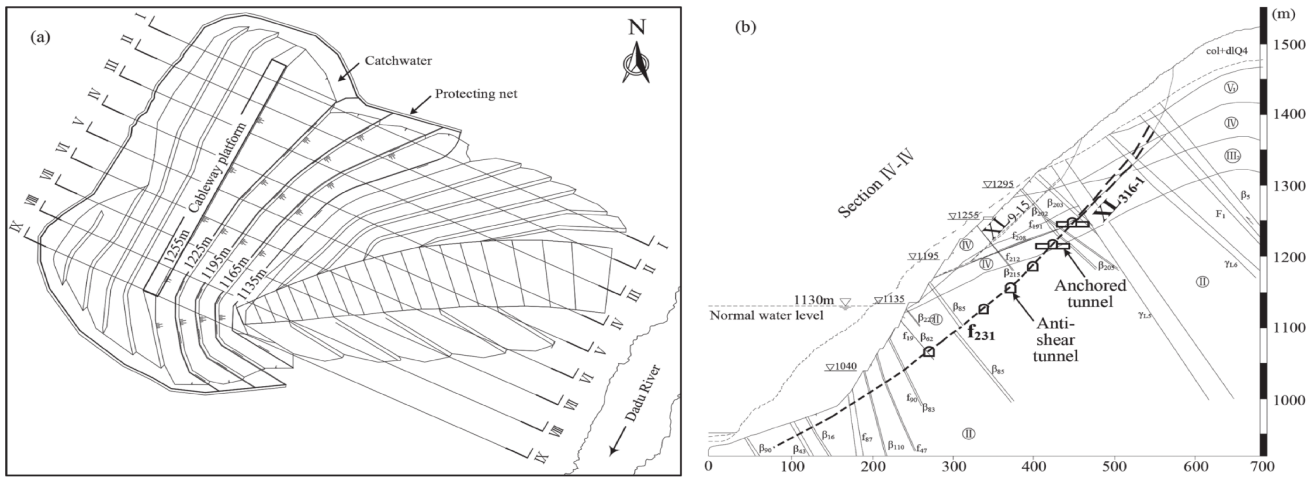

Figure 1. Schematic diagram of Dagangshan right bank slope: (a) excavation outline and (b) geological map of IV-IV section profile.

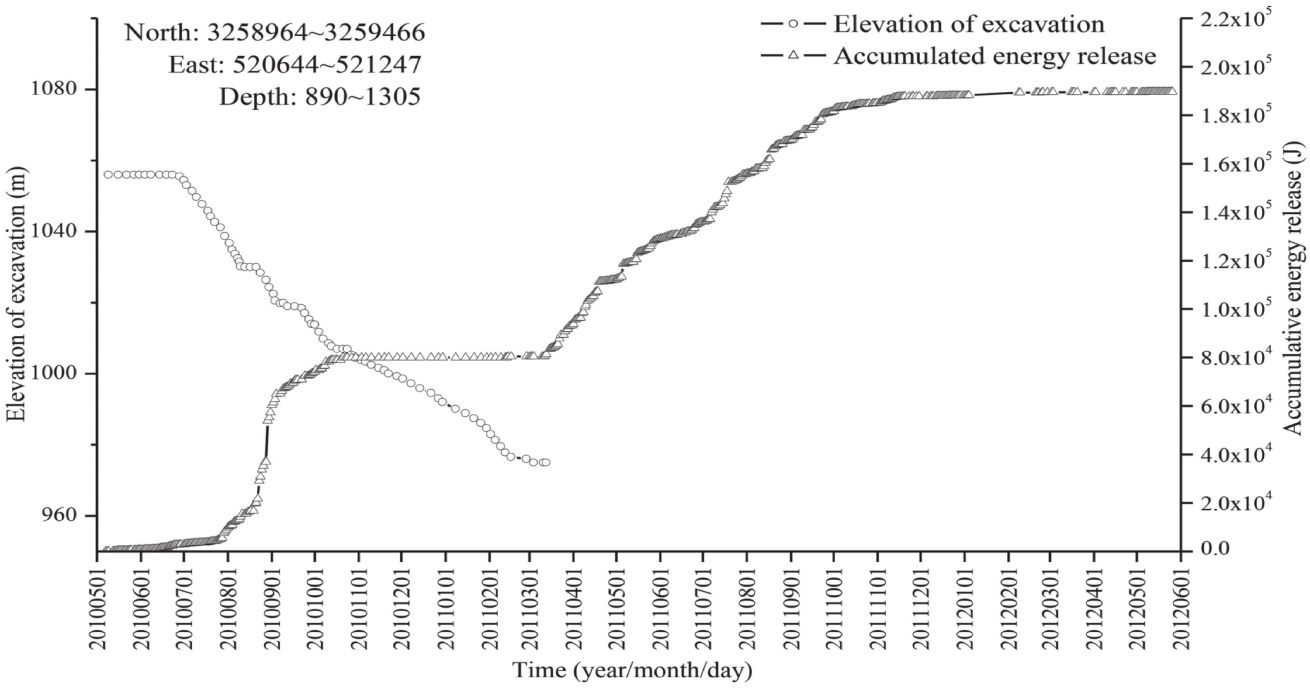

Figure 2. Chart of elevation of slope excavation and accumulative energy release.

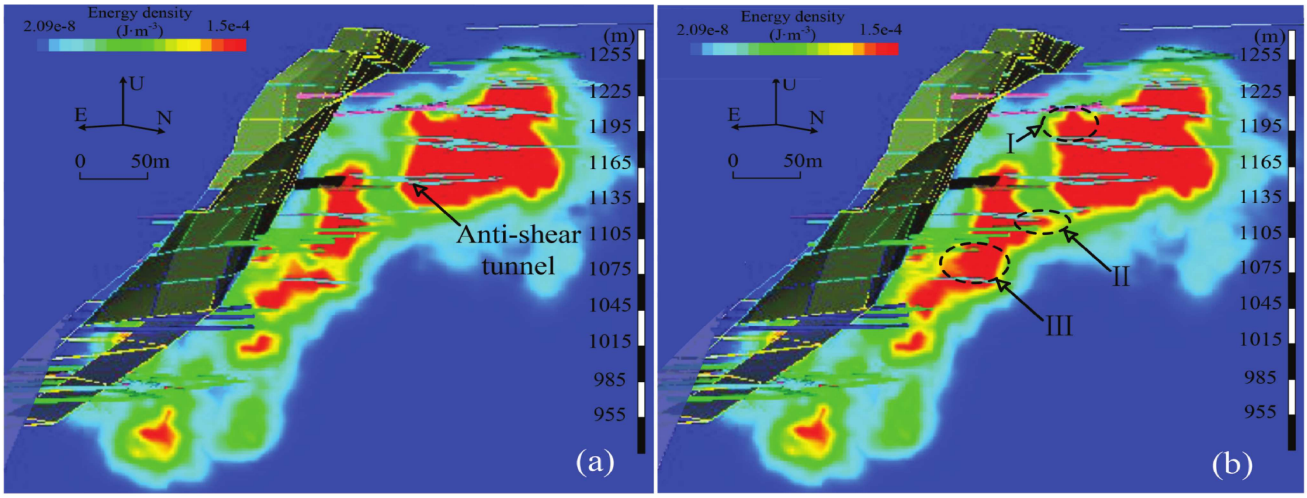

Figure 3. Spatial distribution of microseismic energy density: (a) during excavation and (b) after reinforcement.

system from October 2010 to February 2011, the amount of accumulative energy release increased rapidly prior to November 2011. But the gradient of accumulative energy release curve in August 2010 increased more significantly than that of 2011, which indicates that large-scale slope excavation triggered more high-energy events in this area when excavation restored. According to Figure 3(a), the distribution pattern of high energy release zones is basically consistent with the deep unloading fracture zone XL_{316-1} and the fault f_{231}. The high energy zone was extended to the shear exit of the fault f_{231} at elevation 1060 m (The red area in Fig. 3(a)).

The locations of anti-shear tunnels, major structural planes and geodetic coordinates are projected on the energy density map at the corresponding elevation. As seen from Figure 4(a), during slope excavation, the microseismic energy density was high at elevation 1240 m between two anchored tunnels at the south side of the anti-shear tunnel. The rock mass surrounding the anti-shear tunnel and construction tunnel at elevation 1150 m are the locations for

concentrated microseismic energy release, which is about 60 m from the slope surface (Fig. 4(b)). The high energy density zone at the north side and south-west end of the anti-shear tunnel at elevation 1060 m extends about 40 m and generally along the direction of the anti-shear tunnel (Fig. 4(c)). By comparing Figures 4(a)~4(c), it is found that the distribution of high energy release zones is closely related to the locations of the deep unloading fracture zones XL_{316-1} and the fault f_{231}.

3.3 *Microseismic energy evolution after reinforcement*

After reinforcement by anti-shear tunnels, the accumulative microseismic energy increased slowly (Fig. 5), the high-energy release zones extended by about 10 m into the region at the south side of anti-shear tunnels at elevations 1210 m and 1180 m (I in Fig. 3(b)), the north side of anti-shear tunnel at elevation 1120 m (II in Fig. 3(b)), and the region above elevation 1060 m (III in Fig. 3(b)). These regions were distributed at the edge of anti-shear tunnels and small in area compared to the distribution range of high-energy release zones during excavation, indicating that the stresses in the slope transferred toward the edge of anti-shear tunnels after reinforcement and a small amount of low-energy events were triggered.

Besides, the microseismic energy density at the elevation 1240, 1150 and 1060 m decreased significantly after reinforcement, and the relative high energy release transferred to the edge of anti-shear tunnels and low-threat faults, dikes in the deeper area of the slope. In details, there is no high energy release zone at elevation 1240 m, while relative high energy release transferred to diabase dike (β_{202}) and intersection of anti-shear tunnel and construction tunnel at elevation 1150 m and to diabase dike (β_{202}) and fault f_{167} in the deeper area 200 m away from slope surface at elevation 1060 m, so its mechanical behavior was obviously improved.

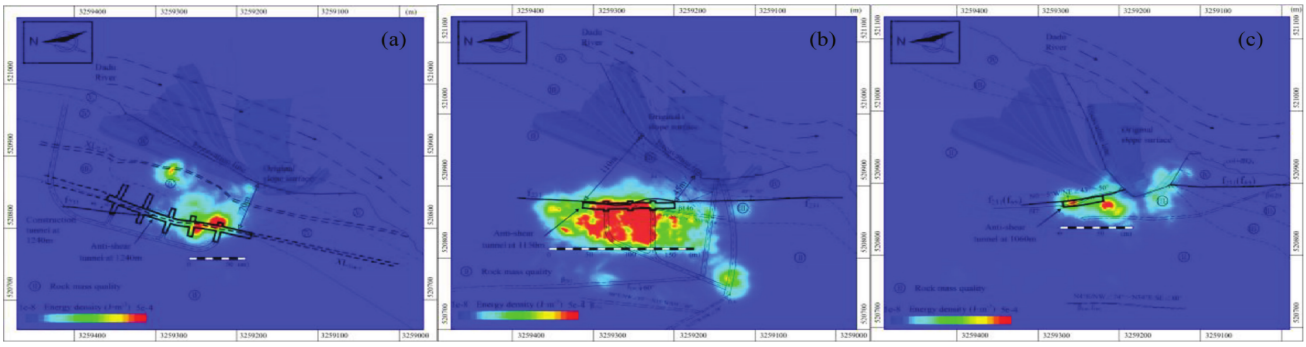

Figure 4. Distribution of microseismic energy density at various elevation levels during excavation: (a) 1240 m; (b) 1150 m; and (c) 1060 m.

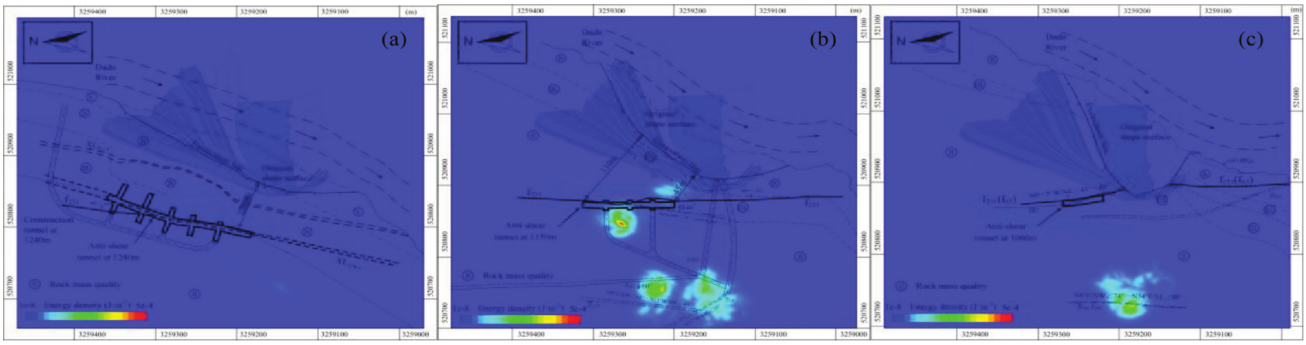

Figure 5. Distribution of microseismic energy density at various elevation levels after reinforcement: (a) 1240 m; (b) 1150 m; and (c) 1060 m.

4 CONCLUSIONS

This study shows that microseismic energy density is a practical index for comprehensively reflecting the location and intensity of micro-cracking in rock mass and analyzing the strain energy storage and release process of rock masses in the microseismic source zone. Potential dangerous area of the slope during exaction and after reinforcement can be determined using microseismic energy density. Due to the disturbance of the unloading fissures XL_{316-1} under slope excavating, high energy density area was induced between two anchored tunnels both south of anti-shear tunnels at elevation 1240 m, while the disturbance of fault f_{231} dipping out of the slope resulted in development of high energy release area along with fault strike at the 1150 and 1060 m elevation, which led to the formation of excavation damage zone extending to about 150 m inside the slope. Microseismic energy density at different elevation decreased significantly after reinforcement, and the relative high energy release transferred to the edge of anti-shear tunnels and low-threat faults, dikes in the deeper area of the slope, which indicates that the anti-shear tunnels played an active role in reinforcement and stress transference, and enhanced the mechanical performance of structural planes. Conclusions can provide references for developing energy criterion and prediction method of high rock slope failure.

REFERENCES

Aki, K. & Richards, P.G. 1980. *Quantitative Seismology: Theory and Methods (Vol I and II)*. San Francisco: W.H. Freeman and Co.

Boatwright, J., & Fletcher, J.B. 1984. The partition of radiated energy between P and S waves. *Bulletin of the Seismological Society of America* 74: 361–376.

Ma, K. 2014. *Study on the Potential Failure Mechanism, Monitoring and Controlling Methods of Rock Slope under Excavation*. PhD Thesis, Dalian University of Technology. (in Chinese).

Mendecki, A.J. 1996. *Seismic Monitoring in Mines*. London: Chapman & Hall: 181–186.

Murphy, M.M., Westman, E.C., Iannacchione, A.T. et al. 2012. Relationship between radiated seismic energy and explosive pressure for controlled methane and coal dust explosions in an underground mine. *Tunnelling and Underground Space Technology* 28: 278–286.

Peng, R.D., Ju, Y., Wang, J.G. et al. 2015. Energy dissipation and release during coall failure under conventional triaxial compression. *Rock Mechanics and Rock Engineering* 48: 509–526.

Snelling, P.E., Laurent, G. & Mckinnon, S.D. 2013. The role of geologic structure and stress in triggering remote seismicity in Creighton Mine, Sudbury. *International Journal of Rock Mechanics and Mining Sciences* 58: 167–179.

Xie, H.P., Ju, Y., Li, L.Y. et al, 2008. Energy mechanism of deformation and failure of rock masses. *Journal of Rock Mechanics and Geotechnical Engineering* 27(9): 1729–1740.

Zhang, Z.Z. & Gao, F. 2015. Confining pressure effect on rock energy. *Chinese Journal of Rock Mechanics and Engineering* 34(1): 1–10. (in Chinese).

Zhang, Z.Z. & Gao, F. 2015. Experimental investigation on the energy evolution of dry and water-saturated red sandstones. *International Journal of Mining Science and Technology* 25(3): 383–388.

Zhang, M.W., Shimada, H., Sasaoka, T. et al. 2013. Seismic energy distribution and hazard assessment in underground coal mines using statistical energy analysis. *International Journal of Rock Mechanics and Mining Sciences* 64: 192–200.